Design and implementation of a scene-dependent dynamically selfadaptable wavefront coding imaging system

Guillem Carles[a,*], Carme Ferran[a], Artur Carnicer[a], Salvador Bosch[a]

[a] *Departament de Física Aplicada i Òptica. Universitat de Barcelona. Martí i Franquès 1, E-08028 Barcelona, Spain.*

Abstract

A computational imaging system based on wavefront coding is presented. Wavefront coding provides an extension of the depth-of-field at the expense of a slight reduction of image quality. This trade-off results from the amount of coding used. By using spatial light modulators, a flexible coding is achieved which permits it to be increased or decreased as needed. In this paper a computational method is proposed for evaluating the output of a wavefront coding imaging system equipped with a spatial light modulator, with the aim of thus making it possible to implement the most suitable coding strength for a given scene. This is achieved in an unsupervised manner, thus the whole system acts as a dynamically selfadaptable imaging system. The program presented here controls the spatial light modulator and the camera, and also processes the images in a synchronised way in order to implement the dynamic system in real time. A prototype of the system was implemented in the laboratory and illustrative examples of the performance are reported in this paper.

Keywords: Imaging Systems, Image Processing, Wavefront Coding, Selfadaptable coding strength
PACS: 42.30.Va, 42.30.Lr, 42.30.Wb

PROGRAM SUMMARY

*Corresponding author.
E-mail address: guillemcarles@ub.edu

Program Title: DynWFC (Dynamic WaveFront Coding)
Journal Reference:
Catalogue identifier:
Licensing provisions: CPC non-profit use license.
Programming language: Labview 8.5 and NI Vision and MinGW C Compiler.
Computer: Tested on PC Intel® Pentium®.
Operating system: Tested on Windows XP.
Classification: 18 Optics
Nature of problem:
The program implements an enhanced wavefront coding imaging system able to adapt the degree of coding to the requirements of a specific scene. The program controls the acquisition by a camera, the display of a spatial light modulator and the image processing operations synchronously. The spatial light modulator is used to implement the phase mask with flexibility given the trade-off between depth-of-field extension and image quality achieved. The action of the program is to evaluate the depth-of-field requirements of the specific scene and subsequently control the codifing established by the spatial light modulator, in real time.

1. Introduction

In optical imaging systems, image quality is affected by an increase of the pupil size which reduces the diffraction limitation (thus increasing imaging resolution) and increases the amount of light entering the system (thus increasing the signal to noise ratio, SNR) but reduces the depth-of-field (DOF) of the imaging system, and the optical aberrations become more severe. To tackle this trade-off, wavefront coding[1] has been proposed. It involves the modification (coding) of the transmitted wavefront by adding a phase function defined at the pupil plane of the optical system. A postdetection image restoration process (decoding) follows to obtain sharp and DOF-extended imagery.

The benefits of the invariance-against-aberrations achieved with the hybrid optical/digital design can be applied in many fields. Many applications may benefit from extended DOF capabilities in macroscopic imaging, for example in surveillance, machine vision or biometrics problems where the DOF extension is a clear advantage [2, 3]; but the technique can also be used to reduce system complexity[4] or for athermalisation and achromatisation of infrared imaging systems[5].

However, the technique has two main drawbacks: noise amplification and

the appearance of artefacts in the restored images[6, 7, 8], which reduce the image quality. Thus the design of wavefront coding systems must take these problems into account, in relation to the required DOF. This is an essential trade-off in the design of such hybrid systems. Moreover, this also emphasises that a single target-DOF design may not be satisfactory for applications in which the required DOF varies, for example if the objects placed in the scene move. Nonetheless, it has been reported that the use of an spatial light modulator (SLM) is adequate to implement the required phase modulation for wavefront coding applications[9]. Hence, the high degree of flexibility provided by the use of the SLM allows on-line adaptation of the applied phase-function to suit the image quality versus DOF extension compromise, given that the latter may vary.

The goal of this work is the design of a computational method, integrating the wavefront-coding framework and other image processing operations, to automatically evaluate the characteristics of a given scene, and subsequently implement a suitable phase-function using an SLM to encode the image formation. The program presented in this paper is thus the implementation of an enhanced wavefront coding imaging system able to adapt its phase coding function to the actual scene requirements, in real time and without supervision.

The paper is organised as follows: Section 2 explains the basic wavefront coding framework. Section 3 describes the method proposed to accomplish the established goals. Section 4 describes the actual programming of the method using the LabVIEW^{TM} language. Section 5 shows the results for an illustrative operation of the system working on the optical bench. Different issues are discussed in section 6 and, finally, the conclusions are presented in section 7.

2. Wavefront coding framework

Wavefront coding is based on the placement of a phase mask (PM) in the aperture stop of an optical system, which modifies the wavefront at the pupil plane. The goal of phase encoding is to achieve both a point-spread function (PSF) that is invariant to different types of aberrations, and a modulation-transfer-function (MTF) that has no nulls within the passband. The latter allows a simple inverse filtering process to restore the acquired encoded images, while the former produces the desired extended DOF (because invariance to defocus aberration is obtained) and allows restoration with a single

filter for all the invariance range.

Several PMs have recently been proposed, and analysed, to produce DOF extension [10, 11, 12, 13, 14, 15]. Among them the most commonly used is the cubic PM, which has a phase function of the form

$$\phi(x_p, y_p) = 2\pi \cdot \alpha \left(x_p^3 + y_p^3\right) \tag{1}$$

where (x_p, y_p) are the normalised pupil coordinates and α determines the PM strength.

This hybrid optical/digital schema has, however, some disadvantages. On the one hand, in terms of spatial-frequency response, the effect of the PM is to reduce the MTF of the imaging system. This unavoidably lowers the SNR of the system since the field formed is captured in the image plane by some noisy sensor. Though different inverse filtering strategies can be used to reduce this effect, the restoration process that reconstructs the MTF (recovering the diffraction limited properties of the system) includes noise amplification in the final images[6, 7]. On the other hand, image quality is also reduced by the appearance of image restoration artefacts due to the mismatch between the actual wavefront that forms the image and the optical-transfer-function (OTF) used in the digital processing stage to restore it[8]. Although the invariance provided by the PM makes this difference small, when applied to scenes with extension, artifacts will appear.

Both effects reduce the resultant image quality and become more problematic as the PM strength increases. Thus a trade-off arises between the amount of DOF extension and the image quality, for a given PM strength. For example, for high α values in Eq. 1 the system is endowed with larger DOFs but the artefacts are more evident and the image quality is poorer. Generally, the trade-off results in an optimum PM strength given the required DOF and the characteristics of the optical system [16, 17, 18].

For example, Fig. 1 shows different implementations of the cubic PM for an optical system with a square pupil, the resulting PSFs and the simulated imaging performances with different amounts of defocus aberration, W_{20}. The value W_{20} is the maximum optical-path error along the pupil plane of the defocus-aberrated wavefront, which has the form $W = W_{20}\left(x_p^2 + y_p^2\right)$. Notice that white noise has been included to simulate the behavior of the camera. It can be seen how a higher coding strength is needed if the defocus aberration is higher, and also how a lower coding strength is desirable if the defocus aberration is reduced. This example illustrates that an optimum PM

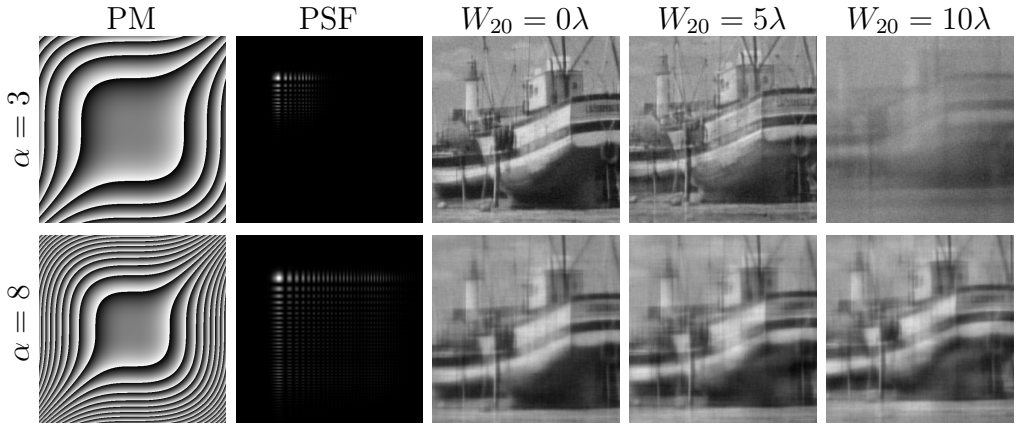

Figure 1: Implementation of a cubic phase mask with $\alpha = 3$ (first row) and $\alpha = 8$ (second row). The images in the different columns show the PM (represented modulo-2π), the PSF of the system and the imaging performance (the restored images) affected by different amounts of defocus, as shown.

strength is obtained depending on the severity of the aberrations.

Finally, as discussed in previous work[9], the use of an SLM as a method of dynamically implementing the desired PM allows for an adaptable coding. The PM is sent to the SLM as a 8-bit VGA resolution image, after 2π-folding the phase function. Thus, a wavefront coding system equipped with an SLM becomes a flexible system, useful if different DOFs are required in different situations.

3. Proposed method

The overall objective of the method proposed is the real-time optimisation of the PM strength in a practical system. To accomplish this, it is fundamental to estimate the amount of defocus present in the imaged scene, and subsequently use this information to select the most suitable PM and implement it by means of an SLM placed at the aperture stop of the optical system. Hence the program has to control the SLM, the camera and perform image processing operations in a synchronised way. The program runs iteratively and the scene is thus constantly evaluated. Hence if the scene changes, the system adapts its coding in real time. This section describes how to accomplish this.

3.1. Calibration

The method proposed here requires different preliminary tasks, which may be considered as the calibration of a given optical system. These tasks are:

1. Choose a list of increasing amounts of defocus aberration. This will be called the list of test amounts of defocus.
2. Acquire and pre-process the PSFs affected by these amounts of defocus. These will be called the set of test PSFs and denoted by T-PSF$_i$, where the index i will be used to identify each PSF within the set.
3. Generate the set of images that implement the PMs of increasing strength. These PMs are supposed to be optimal for each amount of defocus in the list, and account for the trade-off between defocus alleviation and image degradation. See section 3.4 below.
4. Acquire and pre-process the PSFs of the infocus wavefront coding system for each PM generated. These will be called the set of restoring PSFs and analogously denoted by R-PSF$_i$.

3.2. Main operation

The method is an iterative approach divided into the following steps:

1. Acquisition of a wavefront-coded image of the scene with the current PM.
2. Restoration of the image captured in step 1.
3. Acquisition of a conventional image of the scene.
4. Estimation of the amount of defocus from the image in step 3.
5. Update the PM for the defocus aberration detected.

These steps will produce one frame and their iterative repetition will give a real time video output. The general output is the restored image obtained in step 2, the restoration is performed using a parametric Wiener filter. Fig. 2 illustrates the iteration of these steps to constantly select the most suitable PM. The PM used is optimum for the scene at the time of the previous iteration. Hence, if the scene is static the iterations stabilise to the optimum PM.

To select the optimum PM for the actual scene a conventional image (without coding, $\alpha = 0$) is acquired. The amount of defocus is estimated from this image and the selection table pre-calculated in the calibration stage

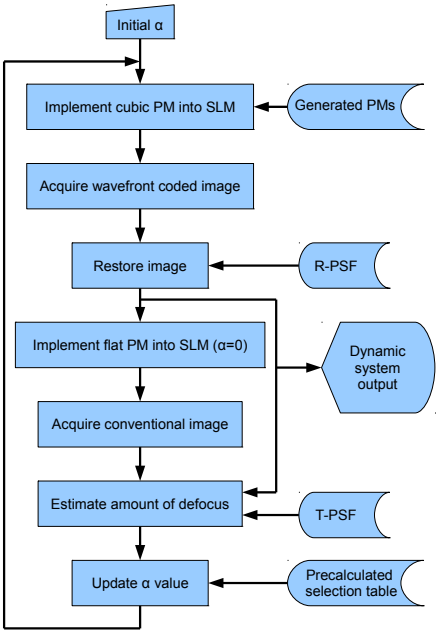

Figure 2: Schema of the iterative functionality of the dynamic system using cubic PMs.

provides the optimum PM directly. Hence, the problem is to determine what amount of defocus in the list of test amounts of defocus best suits the conventional image. The next subsection deals with this problem.

3.3. Defocus estimation

The key issue in the method presented here is the successful determination of the amount of defocus present at the region of interest (ROI) of the scene. The ROI, which is previously established by the user, may be the whole scene or some portion of it. Much work has been published in the field of PSF estimation and blind deconvolution techniques, aimed at tackling the defocus estimation problem[19, 20, 21, 22, 23]. The problem faced here is in fact one of parametric PSF estimation with a single parameter.

Classical techniques for the estimation of defocus, based on identifying the amount of defocus from the position of the zeros of the MTF, are not suitable in this context because the defocus is expected to vary accross the whole image and the ROI (the region from which the defocus must be estimated) may be a little portion of the scene (patch of few pixels) and hence its Fourier transformation will not permit the precise localisation of the zeros.

On the other side, it has been shown how the defocus may also be estimated from the strength of the restoration artefacts within the wavefront coding strength[8]. However, again, this approach is proposed to deal with images affected by uniform defocus, and its reliability will be reduced as the ROI becomes smaller.

The difficulty here is reduced because in this context the defocused image and the wavefront-coded image are both available. A strategy for the estimation of the defocus based on simulations is proposed as follows.

Firstly, the formation of an image of the scene is simulated by the convolution of the restored image R (obtained using the wavefront coding framework and Wiener filtering) and each T-PSF$_i$, to obtain a set of differently degraded images D_i given by

$$D_i[x, y] = \sum_{\forall [p,q]} R[p, q] \cdot T_i[x - p, y - q] \tag{2}$$

If the PM used is adequate for the actual scene, the restored image R is supposed to be defocus-free and hence an accurate reproduction of the scene to some extent. Thus, the set of images D_i will simulate the formation of the image of the scene affected by the different amounts of defocus in the list of test amounts of defocus.

The images D_i are compared to the conventional image acquired, C, (which is obtained without coding, or $\alpha = 0$) to check which defocus aberration value matches with highest similarity. This maximum value will be the estimation of defocus that the conventional image, C, has and which is the goal of this procedure. The similarity evaluation is computed using normalised cross correlation, N,

$$N_{D_i,C}[m, n] = \frac{1}{M - 1} \sum_{\forall [p,q] \in ROI} \frac{\left(D_i[p - m, q - n] - \tilde{D}_i\right)\left(C[p, q] - \tilde{C}\right)}{\sigma_{D_i}\sigma_C} \tag{3}$$

where M is the number of pixels of the two images, $\tilde{D}_i$ and $\tilde{C}$ stand for the mean values of D_i and C respectively, and σ_{D_i} and σ_C stand for the standard deviations of D_i and C respectively. It is essential to account for non-zero displacement values of $[m, n]$ in order to take into account shifting between pixels of the restored image, R, and the conventional capture, C, and thus perform a correct comparison. Among the different values of $N_{D_i,C}$ the maximum is taken; i.e., the final similarity criterion used may be written

$$N_{D_i,C} = \max_{|m|,|n|\leq\gamma} \left[N_{D_i,C}[m,n] \right] \tag{4}$$

where γ is a maximum shifting threshold. Later in section 5, Fig. 8 illustrates this process with an experimental example.

Since wavefront coding applications are typically used to image scenes where the defocus aberration changes across the field of view, it is important to know which region of the image, ROI, the defocus aberration must be estimated from. Actually, it is possible to section the scene, repeat the process for each piece and take the worst case to work on. Moreover, it would also be possible to use this method to track moving object applications where the ROI may change over time.

3.4. Selection table

Once the defocus of the scene has been estimated, the most suitable PM has to be chosen. Choosing the optimum shape and strength of the PM is a design problem that is beyond the scope of this paper. The design may depend on different factors: characteristics of the optical elements in the system, spectral characteristics of the scene, subjective evaluation of the invariance achieved, etc. However, in any case, given a PM shape, its strength will settle the trade-off between the amount of invariance achieved and the image degradation[16]. With this in mind, the proposed method stores and uses a list of different PMs adjusted in some manner to the values in the list of test amounts of defocus. In general terms, it is sufficient to ensure that the list of PMs monotonously increases in the direction of the coding strength.

Each PM generated is actually designed only for the corresponding amount of defocus, but they must also deal well with the higher amounts of defocus up to the next amount on the list, because the same PM will be used until higher values are reached. For the same reason, it is indispensable to set a minimum threshold value for the PM strength in order to have a certain DOF extension, even it is not required in terms of imaging performance.

4. Implementation

The method summarised in Fig. 2 was implemented using LabVIEW^{TM} and its NI Vision library. Fig. 3 shows the Graphical User Interface (GUI) from the program. The program presented here uses a list of test amounts of defocus with 8 different values. Thus the three calibration sets of images

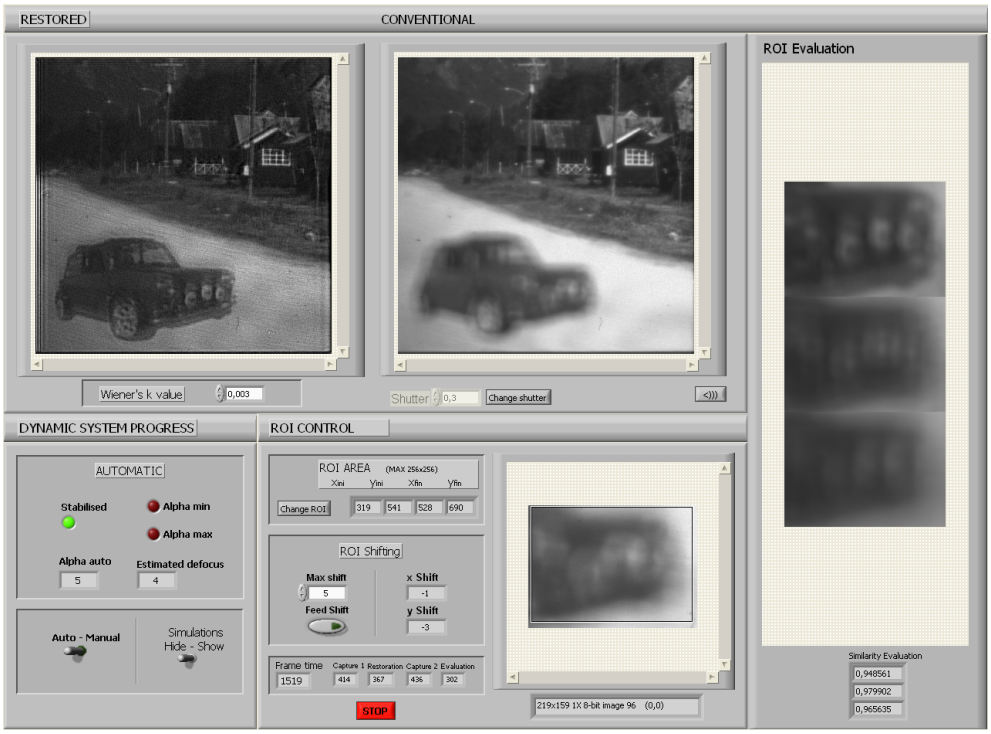

Figure 3: Graphical User Interface of the program.

(T-PSF$_i$, R-PSF$_i$ and PMs) are comprised of 8 images each. The value of the index i (from 0 to 7) indicates at any time which image is being used.

When the program runs, the three sets of images (T-PSF$_i$, R-PSF$_i$ and PMs) are read from the calibration folder and loaded into the memory. Then, the program displays the initial PM on the SLM. To send the required grey-scale image to the SLM, it is plugged to the host computer as a secondary monitor, and it is configured as *extended Desktop* in order to include the SLM resolution in the main display. In this manner, it is enough to indicate the origin coordinate-pixel values where the grey-scale image is to be placed to fill the SLM display.

Once the program is running, the functioning is basically a LabVIEW$^{\text{TM}}$ *flat sequence* of 4 stages implementing sequentially the scheme in Fig. 2. Tab. 1 summarises the essential operations performed in each stage.

In each frame, only three T-PSF$_i$ are evaluated: that corresponding to the present value of the defocus aberration detected within the list of amounts of defocus; that corresponding to the previous value; and that corresponding to

Table 1: Description of the stages of the program in each frame. Note that various operations are performed in each stage because of the data-flow nature of the LabVIEW™ programming language.

Stage	Actions
1	Captures wavefront-coded image. (the PM from the previous iteration is filling the SLM display)
2	Selects the present R-PSF Performs the restoration by Wiener filtering Shows restored image as output at the GUI Sends flat PM to the SLM
3	Captures conventional image Optionally shows conventional image at the GUI
4	Evaluates ROI Increment, maintain or decrement the index i Indicates at the GUI the values of: α corresponding to the updated index i Estimated W_{20} corresponding to the updated index i Calculated displacement values $[m, n]$ Indicates at the GUI whether the system is: stable at a minimum α value at a maximum α value Sends updated PM to the SLM (corresponding to updated index i)

the next value. This corresponds to considering only variations of {-1, 0, +1} in the index i. Using this approach, the system detects whether the coding is too low, too high or just right, and only needs to repeat the operations for three different PSFs. If the estimation of the defocus aberration gives the same value as in the previous iteration, the index i will be unchanged, and so will the PM implemented. In this case, the system stabilises and the flag *Stabilised* in the GUI is activated. Otherwise, the system is not stabilised and the index i will be changed to that corresponding to the T-PSF$_i$ that produces greatest similarity. In this case, the three PSFs used in the calculations in the next iteration will be shifted towards PSFs producing higher similarity. This schema means that the system evolves since the most suitable PM within the set of generated PMs is found for the given scene; i.e., the system evolves until it becomes stable.

The evaluation procedure involves using Eq. (4) over the three PSFs tested to identify which best suits the conventional image C. To speed up the calculation of Eq. (4), the code has been written in C and an external DLL is generated. The output of this function is the calculation of the normalised crosscorrelation for a limited displacement range of $|m|, |n| \leq \gamma$ (i.e. a number of $(2\gamma + 1)^2$ times) and the values of the indices $[m, n]$ that produce the

highest correlation. The main program calls this DLL to compare the captured conventional image C and the convoluted image D_i. Then, the main program uses the same displacement values $[m, n]$ to evaluate D_{i+1} and D_{i-1} using Eq. (3) directly. Finally the evaluation (over the three performed) with greatest similarity indicates whether the index i must be incremented, maintained or decreased. A schematic representation of the defocus estimation procedure is shown in Fig. 4.

The maximum threshold shift in the calculations (the value of γ) must be higher than the real shift between the conventional image C and the restored wavefront-coded image R. This means that high γ values are necessary, which at the same time increases the evaluation time (note that the burden of calculating Eq. (4) increases quadratically with γ). In order to reduce the computations, the shifting values $[m^*, n^*]$ that result from one iteration are fed back in the next iteration and the calculation of Eq. (4) is not performed for the ranges $(-\gamma \leq m \leq \gamma)$ and $(-\gamma \leq n \leq \gamma)$ but for the ranges $(m^* - \gamma \leq m \leq m^* + \gamma)$ and $(n^* - \gamma \leq n \leq n^* + \gamma)$. This fact reduces the required γ value because with this modification γ only needs to cope with the *difference* in displacement produced by two consecutive PMs, instead of the absolute displacement. This feedback might produce erroneous results if the exact displacement is lost or erroneously calculated, but in that case, it suffices to reset the indices to zero and let the system stabilise again. It is possible to enable/disable this feedback in the GUI, as well as to set the value of γ.

The value of the index i may not reach the extreme values, because the evaluation process always has to operate on three indices. For this reason the flags *Alpha-min* and *Alpha-max* seen in Fig. 3 are implemented in the GUI. The former corresponds to keeping $i = 1$ even if the evaluation requires it to be reduced, while the latter corresponds to keeping $i = 6$ (in the case of a list of 8 items) even if the evaluation requires it to be increased.

An additional feature of the program is the possibility of disabling the whole evaluation process and using the system with a manually selected PM (from the PMs loaded in the list), as seen in Fig. 3. This corresponds to a wavefront coding system working in real time, without any evaluation. It corresponds to the operation using only stages 1 and 2 (and optionally 3 if desired, but it would no longer be necessary) of Tab. 1.

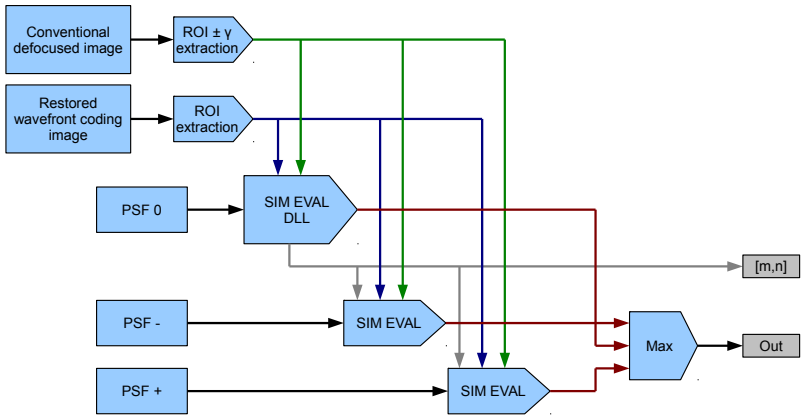

Figure 4: Schema of the similarity evaluation computation. The box "SIM EVAL DLL" stands for the calculus of Eq. (4) using the dll, and the boxes "SIM EVAL" stand for the normalised correlation, Eq. (3), using the indices $[m, n]$ from the former.

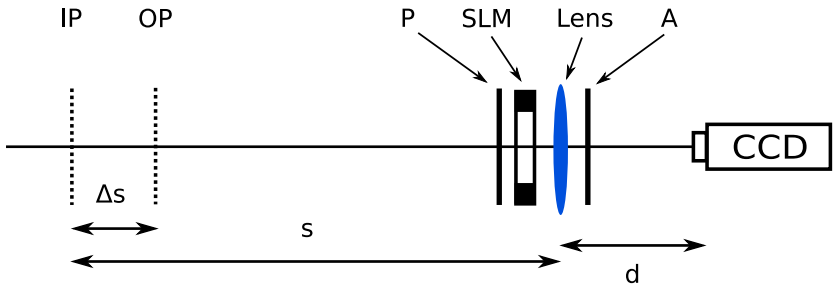

Figure 5: Layout of the optical system, composed of a camera, a lens, an SLM and two polarisers. A: analyser, P: polariser, IP: Infocus plane, OP: Out-of-focus plane, Δs: longitudinal defocus.

5. Experimental illustration

The method has been experimentally implemented with an optical system set in the laboratory. Its layout is plotted in Fig. 5. A liquid crystal display extracted from an Epson projector was used as the SLM to implement the PMs. A previous calibration procedure is needed to obtain the relation between grey level (in the image sent through the VGA signal) and the actual phase added to the transmitted wavefront[9]. Once this calibration has been performed, the actual modulation is directly chosen from the image sent to the SLM.

The aperture stop of this optical system is the SLM itself, which has a

Table 2: Values of the defocus aberration, W_{20} and the α parameter for acquiring the sets of R-PSF$_i$, R-PFS$_i$ and generating the set of PMs.

Index i	Defocus W_{20}/λ	Cubic PM α
0	0	0
1	1	1
2	2	3
3	4	5
4	6	7
5	8	9
6	10	11
7	12	13

rectangular shape. The calibration values used are shown in Tab. 2. The set of images implementing cubic PMs were generated and the sets {T-PSF} and {R-PSF} for the optical system were acquired, pre-processed and stored. All for each value in Tab. 2.

Fig. 6 shows the sequential frames of an example which illustrates the working performance. A particular scene was set composed of a background (the landscape with houses) situated at the IP plane indicated in Fig. 5 and a particular object (the car) situated at the OP plane indicated in Fig. 5. The ROI is defined to include mainly the object. The configuration is made so as to leave the background static and the object movable. Thus the object is the only part in the field of view which is affected by defocus aberration. The first frame, Fig. 6(a), corresponds to a stabilised initial state of $\alpha = 3$, and the defocus aberration of the ROI is approximately $W_{20} = 2\lambda$. Then the object was moved further from the infocus plane increasing the defocus aberration until $W_{20} = 6\lambda$, as seen in the frame in Fig. 6(b) (where it can be seen how the coding is not sufficient). A few frames later, the system stabilises at $\alpha = 7$, as seen in the frame in Fig. 6(c). Frames in Fig. 6(d)-(e) show the stabilisation for even greater defocus: they correspond to approximately $W_{20} = 10\lambda$, Fig. 6(d) corresponds to $\alpha = 7$ (which is too low) and the system increases the PM strength to $\alpha = 11$ as seen in Fig. 6(e). The images on the bottom are the output of the conventional system (without wavefront coding) and are shown for clarity. Thus, Fig. 6 as a whole shows how the system increases the PM strength if the ROI in the scene becomes more defocused in order to further extend the DOF.

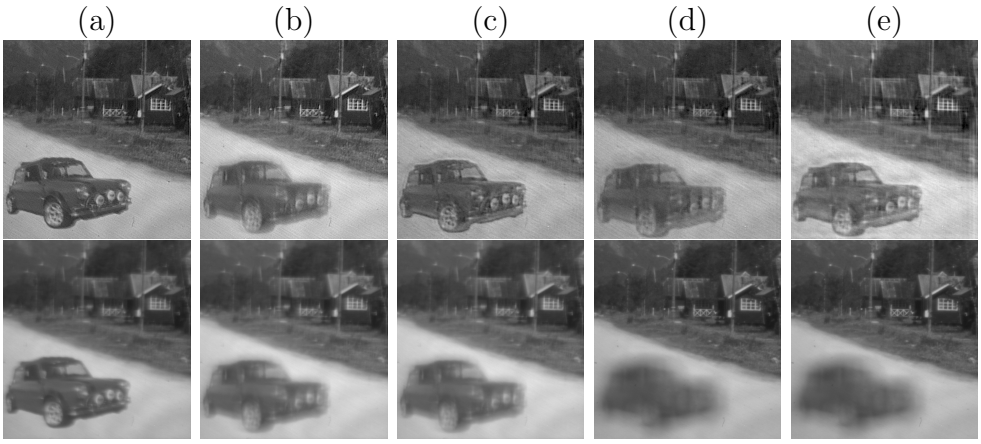

Figure 6: Selected frames from a working sequence showing how the system increases the coding strength if the amount of defocus increases. The system is (a) initially stable at $W_{20} = 2\lambda$ and $\alpha = 3$, then the object is moved away from the infocus plane becoming more defocused and the system is (b) not stable at $W_{20} = 6\lambda$ and $\alpha = 3$, then the system changes the PM (increasing its strength) until it is (c) stable at at $W_{20} = 6\lambda$ and $\alpha = 7$, then the ROI is even more defocused and the system is (d) not stable at $W_{20} = 10\lambda$ and $\alpha = 7$, and finally the system changes the PM (increasing its strength) until it is (e) stable again at $W_{20} = 10\lambda$ and $\alpha = 11$.

Fig. 7 shows an analogous cycle but in decreasing defocus steps. Fig. 7 shows how the system reduces the PM strength in order to obtain better image quality if large DOFs are no longer required. Both Fig. 6 and Fig. 7 correspond to an unsupervised action of the proposed system. The experiments clearly show the system trend towards the desired PM strength.

To further illustrate the evaluation process, Fig. 8 shows the illustrative images involved in a working example. It can be seen that the amount of defocus is well identified, coping with the shift between the conventional image and the restored image.

The final speed of the system depends on many factors: value of γ, size of the ROI, acquisition time of the images. Using a typical current PC (Intel® Pentium® 4 processor at 3.2 GHz with 1 GB RAM), the speed achieved in different combination cases is shown in Tab. 3.

6. Discussion

The dynamic system proposed in this paper is intended to evolve to find the most suitable PM for a given scene. The method would fail if the

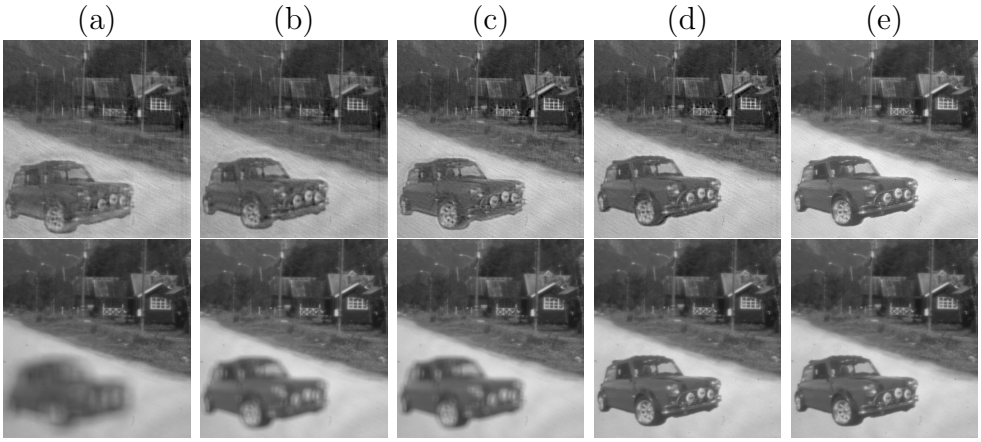

Figure 7: Selected frames from a working sequence showing how the system decreases the coding strength if the amount of defocus decreases. The system is (a) initially stable at $W_{20} = 8\lambda$ and $\alpha = 9$, then the ROI is moved to the infocus plane reducing the defocus aberration and the system is (b) not stable at $W_{20} = 4\lambda$ and $\alpha = 9$, then the system changes the PM (reducing its strength) until it is (c) stable at at $W_{20} = 4\lambda$ and $\alpha = 5$, then the ROI is moved at the infocus plane and the system is (d) not stable at $W_{20} = 0\lambda$ and $\alpha = 5$, and finally the system changes the PM (reducing its strength) until it is (e) stable again at $W_{20} = 0\lambda$ and $\alpha = 1$.

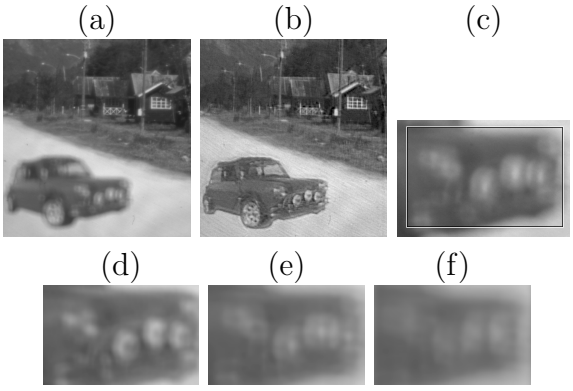

Figure 8: Evaluation example. (a) Conventional image with approximately $W_{20} = 4\lambda$ of defocus aberration in the ROI. (b) Restored output of the wavefront coding system using a cubic PM with $\alpha = 5$ and the parametric Wiener filter. (c) γ-extended ROI of (a) with a frame showing the actual ROI used in the calculations (coping with the displacement between (a) and (b)). (d)-(f) Convolution of (b) with the testing PSFs with $W_{20} = 2\lambda$, $W_{20} = 4\lambda$ and $W_{20} = 6\lambda$ respectively. At the bottom are the similarity evaluation values for each of the testing PSFs using Eq. (4). As seen, the maximum similarity effectively identifies the defocus aberration.

Table 3: Tested speed of the dynamic system with different significant cases, using a typical current PC (Intel® Pentium® 4 processor at 3.2 GHz with 1 GB RAM). The last rows correspond to disabling the evaluation procedure.

ROI (pixels)	γ (pixels)	Exposure (ms)	Frame time (ms)
100×100	5	300	1465
100×100	5	20	765
100×100	10	300	1503
100×100	10	20	906
200×200	5	300	1565
200×200	5	20	966
200×200	10	300	2334
200×200	10	20	1728
—	—	300	800
—	—	20	496

wavefront-coded image obtained during one iteration were not defocus-free. Thus, if the scene suffers a sudden increase of the defocus aberration, the PM initially used in the iteration will be too low and will not be able to encode that amount of aberration. If that occurs, the restored image R will be affected by defocus and hence the image formation simulation will not be correct, leading to erroneous defocus estimation. This can be avoided by considering sufficiently slow variations of growing defocus aberrations, or by achieving enough speed in the digital processing component of the hybrid system. In other words, changes in the amount of defocus aberration at the scene must be slow enough as to be *followed* by the proposed dynamic system.

Since the system action is dependent on the scene, it is very important to set the ROI properly. For instance, if the ROI does not have finer enough details it will not be possible to detect a defocus aberration below a certain value. This is due to the low-pass nature of Eq. (2): it will only be meaningful if the ROI does indeed have higher frequency content to be filtered by the convolution operation. In other words, the ROI should show details smaller than the testing PSFs in order to manifest differences within them. If this condition is not fulfilled, the system becomes falsely stabilised, because the defocus estimation procedure gives an incorrect result due to the use of inadequate content in the ROI of the scene.

The amounts of defocus in the list are not crucial but relevant. If there are too many steps in the list the PSFs will not differ enough to make the simi-

larity evaluation significant. On the other hand, a minimum number of steps is needed so as to permit each PM to properly encode every range between consecutive values. In practice, steps in the order of one/two wavelengths work fine.

It is also worth mentioning that in the normal operation of the system, those actual amounts of defocus for which each change of PM takes place, are likely to slightly differ from the ones in the list, due to a particular frequency content in the ROI. But this fact is incidental because the final goal is not to know the exact amount of defocus present in the captured image, and the dynamic system works well regardless of this mismatch between the actual and the estimated amounts of defocus. In this sense the dynamic system turns out to be highly robust.

There is a wide variety of applications which may benefit from the system proposed. Applications ranging from surveillance, machine vision, robotic target detection or tracking objects applications may significantly encounter DOF variations in their imaged targets. These kind of applications may accept the restriction of using monochromatic light, which has been assumed through this paper. This assumption is of importance because of the modulo-2π implementation of the phase encoding function. If the monochromatic restriction is not fulfilled a wavelength-related blurring in the formed images will impact and reduce the final image sharpness of the system; however, it is not expected a dramatic reduction of the system performance.

7. Conclusions

A computational imaging system based on wavefront coding has been presented. The system estimates the amount of defocus aberration present in a given scene and implements an appropriate PM using an SLM, in an unsupervised manner. Since this is done iteratively, the system detects changes in the defocus aberration in the scene and dynamically adapts the PM to them. The method is implemented using LabVIEW$^{\text{TM}}$ and a custom made dll written in C to calculate Eq. (4). An optical system was set in the laboratory to test the program and illustrative examples are reported showing the successful performance of the method.

Acknowledgements

This paper has been supported in part by the CICYT (the Spanish R+D Agency) project DPI2008-04175. Guillem Carles gratefully acknowledges the

financial support of FPI grant BES-2006-12357 from the Spanish Ministry of Science and Innovation.

[1] J. Edward R. Dowski, W. T. Cathey, Extended depth of field through wave-front coding, Appl Optics 34 (11) (1995) 1859–1866.

[2] W. Cathey, E. Dowski, New paradigm for imaging systems, Appl Optics 41 (29) (2002) 6080–6092.

[3] R. Narayanswamy, G. Johnson, P. X. Silveira, H. Wach, Extending the imaging volume for biometric iris recognition, Appl Optics 44 (5) (2005) 701–712.

[4] M. Demenikov, E. Findlay, A. R. Harvey, Miniaturization of zoom lenses with a single moving element, Opt. Express 17 (8) (2009) 6118–6127.

[5] G. Muyo, A. Singh, M. Andersson, D. Huckridge, A. Wood, A. R. Harvey, Infrared imaging with a wavefront-coded singlet lens, Opt. Express 17 (23) (2009) 21118–21123.

[6] S. Sherif, E. Dowski, W. Cathey, Effect of detector noise in incoherent hybrid imaging systems, Opt Lett 30 (19) (2005) 2566–2568.

[7] J. van der Gracht, J. G. Nagy, V. Pauca, R. J. Plemmons, Iterative restoration of wavefront coded imagery for focus invariance, in: Integrated Computational Imaging Systems, Optical Society of America, 2001, p. ITuA1.

[8] M. Demenikov, A. R. Harvey, Image artifacts in hybrid imaging systems with a cubic phase mask, Opt. Express 18 (8) (2010) 8207–8212.

[9] G. Carles, G. Muyo, S. Bosch, A. R. Harvey, Use of a spatial light modulator as an adaptable phase mask for wavefront coding, Journal of Modern Optics 57 (10) (2010) 893–900.

[10] K. Kubala, E. Dowski, W. Cathey, Reducing complexity in computational imaging systems, Opt Express 11 (18) (2003) 2102–2108.

[11] S. Prasad, T. Torgersen, V. Pauca, R. Plemmons, J. van der Gracht, High-resolution imaging using integrated optical systems, Int J Imag Syst Tech 14 (2) (2004) 67–74.

[12] S. Mezouari, A. Harvey, Phase pupil functions for reduction of defocus and spherical aberrations, Opt Lett 28 (10) (2003) 771–773.

[13] S. Sherif, W. Cathey, E. Dowski, Phase plate to extend the depth of field of incoherent hybrid imaging systems, Appl Optics 43 (13) (2004) 2709–2721.

[14] A. Castro, J. Ojeda-Castaneda, Asymmetric phase masks for extended depth of field, Appl Optics 43 (17) (2004) 3474–3479.

[15] Q. Yang, L. Liu, H. Sun, Optimized phase pupil masks for extended depths of field, Opt Commun 272 (1) (2007) 56–66.

[16] G. Carles, A. Carnicer, S. Bosch, Phase mask selection in wavefront coding systems: a design approach, Opt Laser Eng 48 (7-8) (2010) 779–785.

[17] G. Muyo, A. Harvey, Decomposition of the optical transfer function: wavefront coding imaging systems, Opt Lett 30 (20) (2005) 2715–2717.

[18] C. Pan, J. Chen, R. Zhang, S. Zhuang, Extension ratio of depth of field by wavefront coding method, Opt. Express 16 (17) (2008) 13364–13371.

[19] T. Cannon, Blind deconvolution of spatially invariant image blurs with phase, IEEE Trans Acoust Speech Signal Process 24 (1) (1976) 58–63.

[20] G. R. Ayers, J. C. Dainty, Iterative blind deconvolution method and its applications, Opt Lett 13 (7) (1988) 547–549.

[21] M. Chang, A. Tekalp, A. Erdem, Blur identification using the bispectrum, IEEE Trans Signal Process 39 (10) (1991) 2323–2325.

[22] N. Miura, K. Ohsawa, N. Baba, Single-frame blind deconvolution by means of frame segmentation, Opt Lett 19 (10) (1994) 695–697.

[23] J. Lin, C. Zhang, Q. Shi, Estimating the amount of defocus through a wavelet transform approach, Pattern Recogn Lett 25 (4) (2004) 407–411.